LANGMUIR

pubs.acs.org/Langmuir Article

Inorganic Nanoparticles Embedded in Polydimethylsiloxane Nanodroplets

Sandrine Lteif, Neda A. Nosratabad, Sisi Wang, Yan Xin, Steven J. Weigand, Hedi Mattoussi, and Joseph B. Schlenoff*

Cite This: *Langmuir* 2023, 39, 15748−15755 Read Online

ACCESS | Metrics & More | Article Recommendations | Supporting Information

ABSTRACT: To stabilize and transport them through complex systems, nanoparticles are often encapsulated in polymeric nanocarriers, which are tailored to specific environments. For example, a hydrophilic polymer capsule maintains the circulation and stability of nanoparticles in aqueous environments. A more highly designed nanocarrier might have a hydrophobic core and a hydrophilic shell to allow the transport of hydrophobic nanoparticles and pharmaceuticals through physiological media. Polydimethylsiloxane, PDMS, is a hydrophobic material in a liquid-like state at room temperature. The preparation of stable, aqueous dispersions of PDMS droplets in water is problematic due to the intense mismatch in surface energies between PDMS and water. The present work describes the encapsulation of hydrophobic metal and metal oxide nanoparticles within PDMS nanodroplets using flash nanoprecipitation. The PDMS is terminated by amino groups, and the nanodroplet is capped with a layer of poly(styrenesulfonate), forming a glassy outer shell. The hydrophobic nanoparticles nucleate PDMS droplet formation, decreasing the droplet size. The resulting nanocomposite nanodroplets are stable in aqueous salt solutions without the use of surfactants. The hierarchical structuring, elucidated with small-angle X-ray scattering, offers a new platform for the isolation and transport of hydrophobic molecules and nanoparticles through aqueous systems.

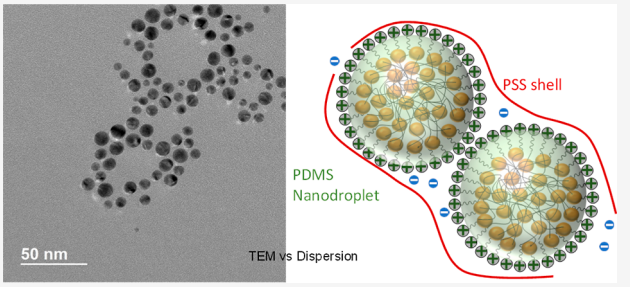

INTRODUCTION

Colloidal nanocarriers have been under intense investigation for their use in drug delivery and imaging applications. Carriers, such as liposomes, polymer vesicles, and micellar dispersions, have shown great potential in solubilizing hydrophobic drugs.[1,2] Polymer nanodroplets offer enhanced synthetic versatility, drug loading capacity, stability, and biocompatibility.[2−5] Combinations with inorganic contrast agents having a metallic core, such as gold nanoparticles (AuNPs), are promising contenders for biomedical imaging.[3,6,7] Most of these applications require working in aqueous media, which can be problematic for hydrophobic nanoparticles, since they are susceptible to aggregation in aqueous solutions.[6,8,9] Encapsulation of these hydrophobic nanoparticles within a water-soluble vehicle has also been a challenge.[2]

In aqueous solutions, self-assembled block copolymer nanoparticles are stabilized with a hydrophilic shell. This shell forms a corona when in contact with water, providing stability to the hydrophobic core that increases the solubility of encapsulated materials.[10−13] Because of their synthetic flexibility, polymeric nanodroplets have attracted interest, with preparation falling into three general areas.[14] The first is dispersing the preformed polymer by emulsification;[15,16] the second is a solvent evaporation method;[17] and finally, nanoprecipitation is employed.[5,14] Polystyrene-*block*-poly(ethylene oxide) micelles loaded with quantum dots, gold and iron oxide nanoparticles were prepared as emulsions by Bae et al.[18] The solvent evaporation method was used to prepare quantum dots encapsulated in phospholipid-based micelles.[19,20] However, these types of micelles tend to have limited stability and a low limit of drug loading.

Flash nanoprecipitation (FNP) to encapsulate hydrophobic organic additives was studied extensively by Johnson and Prud'homme.[21] FNP relies on rapid mixing between solvent and nonsolvent and instantaneous dilution to prevent aggregation. This can be achieved with a confined impinging jet (CIJ) or a multi-inlet vortex mixer, where mixing and precipitation take less than a couple of seconds.[22,23] FNP has been exploited to make multicomponent composite nanoparticles (CNPs) as kinetically stabilized nanoscale carriers.[3,21,24,25] Copolymers based on poly(ethylene glycol), PEG, and a multi-inlet vortex mixer have been used to

Received: August 11, 2023
Revised: September 29, 2023
Accepted: October 10, 2023
Published: October 26, 2023

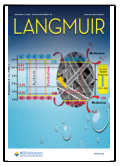

encapsulate a variety of species, such as gold nanoparticles,[3] fluorescent nanoparticles,[26−28] paclitaxel,[29] β-carotene, and polyethylenimine.[3,30] PEG, a popular candidate for nanocarriers because of its biocompatibility and noncytotoxicity, has been copolymerized with polystyrene,[10,18,27,31] poly(caprolactone), PCL,[26,32] poly(lactic acid), PLA,[32,33] and poly(lactic-*co*-glycolic acid), PLGA.[23,32,34,35] However, PLA particles showed limited stability,[33] and PCL particles were not stable.[26,33] PEG-*b*-PLGA showed the highest stability due to the drastic difference in solubility between the two blocks and the fact that the glass transition temperature, T_g, for PLGA is near ambient conditions.[23,34] Pustulka et al. concluded that the nanoparticle is primarily stabilized by the hydrophobic block, which requires a T_g higher than room temperature.[23] Glassy hydrophobic polymers have been the leading choice for the core, especially when the core volume is greater than that of the shell.[36]

Compared to PMMA and PCL, PLGA nanoparticles formed by nanoprecipitation encapsulated dyes, which aggregated more strongly.[37] PCL and PMMA undergo fast nanoprecipitation, and the dye is incorporated during particle growth, while in the case of PLGA, the dye is embedded within the polymer nuclei or participates in particle formation.[37] These particles were stabilized in biological media by anionic surfactants.[38]

Liquid like polymers such as poly(dimethylsiloxane), PDMS, have rarely been used for nanocarriers, despite the extensive use of this material for biomedical applications. Because unmodified PDMS nanoparticles tend to aggregate in solution, they are usually either copolymerized[39,40] or their backbone is altered.[41] Cross-linking also stabilizes particles and larger articles of PDMS, forming "silicone rubber." We have recently reported the formation of stable nanoparticles without cross-linking from PDMS with positive end groups by FNP.[42]

Here, we report on the use of an ammonium-terminated polydimethylsiloxane to encapsulate a high loading of inorganic nanoparticles such as gold, iron oxide, and silica via FNP. FNP provided a fast and simple process to produce colloidally stable hybrid nanoparticles. The highly hydrophobic, nontoxic, and biocompatible PDMS provided means for dissolving water-insoluble compounds. The stability of these particles in an aqueous solution was enhanced by introducing a glassy poly(styrenesulfonate) shell, discussed in detail in our previous work.[42]

EXPERIMENTAL SECTION

Materials. Chloroform, hexane, gold(III) chloride trihydrate (>99.9%), oleylamine (70%), oleic acid, iron(III) chloride hexahydrate, 1-octadecene, and trifluoromethanesulfonic (tiflic) acid were from Sigma-Aldrich. Deuterated chloroform ($CDCl_3$) was purchased from Cambridge Isotope Laboratories. Ethanol and HPLC-grade water were from VWR Chemicals. Magnesium sulfate anhydrous was from Fisher Scientific. Polydimethylsiloxane terminated with aminopropyl groups at both ends (10−15 cST, nominal molecular weight of 900 g mol^{-1}, PDMS-NH_2) was obtained from Gelest. Polystyrenesulfonate, sodium salt (PSS, 16,000 g mol^{-1}) was from Scientific Polymer Products. Hydrophobically modified silica nanoparticle (particle size 10−15 nm) colloidal solution in isopropanol (IPA) were a gift from Nissan Chemical.

Protonation of PDMS-NH_2. The amine-terminated polydimethylsiloxane was protonated following a literature procedure.[42] ^{1}H NMR (600 MHz, chloroform-*d*): δ 6.82 (s, 6H), 3.03−2.92 (m, 4H), 1.76−1.63 (m, 4H), 0.59−0.53 (m, 4H), 0.18−0.01 (m, 117H).[42]

Oleylamine-Capped AuNPs (OLA-AuNPs). The oleylamine-capped AuNPs (∼10 nm in diameter measured by TEM) were prepared by rapidly injecting gold precursor into a preheated oleylamine solution.[43] Briefly, 119 mg of gold(III) chloride trihydrate dissolved in 2 mL of oleylamine was rapidly injected into 4 mL of oleylamine in a 50 mL three-neck round-bottom flask at 150 °C under N_2. The heating was continued at 150 °C for 40 min. The solution was then cooled to room temperature and then centrifuged at 3700 rpm for 15 min to remove unreacted precursors. The supernatant was collected and diluted in hexane.

Iron Oxide Nanoparticles (IONPs). Oleic acid-capped IONPs (16 nm in diameter measured by TEM) were synthesized using the thermal decomposition of iron-oleate precursors at high temperatures following the procedure reported by Hyeon and co-workers.[44] To prepare the oleate precursor, 3.6 g of $FeCl_3{\cdot}6H_2O$ and 12.5 g of sodium oleate were dissolved in a mixture of 26 mL of ethanol, 20 mL of water, and 46 mL of hexane. The mixture was heated to 70 °C and left at that temperature for 4 h. The iron-oleate complex was washed with water three times. The solvent was evaporated, yielding an iron-oleate complex as a brown oil. 3.6 g of the iron oleate complex and 0.57 g of oleic acid were dissolved in 20 g of 1-octadecene. The mixture was heated to 320 °C under N_2 at a heating rate of 3.3 °C min^{-1}, and then maintained at that temperature for 30 min. A brownish-black color developed, indicating the formation of iron oxide nanoparticles. The resulting NP dispersion was centrifuged (3700 rpm for 15 min).

PDMS Nanodroplet Preparation. All inorganic/polymer nanodroplet solutions (Au-PDMS-NH_3^+, Au-PDMS-NH_3^+PSS, IONP-PDMS-NH_3^+, and SiO_2NP-PDMS-NH_3^+) were prepared by FNP using a hand-operated CIJ using a design reported previously (Figure S1).[42] 4 mg of AuNP, dried from hexane, was redispersed in 0.5 mL THF. The AuNP solution was added to 25 mg of PDMS-NH_3^+ in 12.5 mL of THF. The inorganic/polymer solution in THF was transferred to a syringe while another syringe had the same volume of water (nonsolvent). Both syringes were actuated simultaneously, and the effluent, 25 mL at a rate of about 5 mL s^{-1}, was immediately precipitated into a reservoir of water (225 mL) containing 15 mg PSS to deposit a stabilizing shell of PSS on the nanodroplet of PDMS-NH_3^+. The same process was repeated to form IONP-PDMS-NH_3^+ NPs with an IONP concentration of 0.032 mg mL^{-1}. For the SiO_2-PDMS-NH_3^+, the SiO_2 NPs were dispersed in isopropyl alcohol and then redispersed in THF to yield a final SiO_2 NP concentration of 0.016 mg mL^{-1}.

Dynamic Light Scattering. A goniometer system (ALV CGS-3-A0-11) equipped with a vertically polarized He−Ne laser (λ = 632.8 nm, 22 mW) was used to determine the size and stability of the nanodroplets in solution. Two mL of each solution was filtered through a 0.45 μm filter and transferred to capped cylindrical borosilicate tubes (10 mm optical path). Measurements were taken on freshly prepared samples (at t = 0) and 24 h later at a fixed scattering angle of 90° at room temperature through a reservoir filled with a refractive index matching fluid (toluene). All aqueous inorganic-polymer nanodroplet solutions were passed through a 0.45 μm filter and had a PDMS-NH_3^+ concentration of 0.1 mg mL^{-1}, while the concentration of the inorganic nanoparticles varied as follows: [AuNP] 0.016 mg mL^{-1}, [IONP] 0.032 mg mL^{-1}, and [SiO_2 NP] 0.016 mg mL^{-1}. For Au-PDMS-NH_3^+PSS, the PSS concentration was 0.06 mg mL^{-1}. ALV correlator software V.3.0 was used to obtain the intensity autocorrelation function $g^{(2)}(q,\tau)$ where $q = 4\pi n_D \sin(\theta/2)/\lambda$ by pseudocross-correlation of the signal from an avalanche photodiode.

UV−Vis Absorbance. The stability of the Au-NPs in Au-PDMS-NH_3^+ and Au-PDMS-NH_3^+PSS nanodroplet solutions was determined by using UV−vis absorption spectra (Cary 100 Bio, Varian). The Au-NP surface plasmon resonance (SPR) of the nanodroplet suspensions at around 520 nm was measured for freshly prepared samples and also after 24 h using Au-PDMS-NH_3^+ (0.1 mg mL^{-1} PDMS-NH_3^+ and 0.016 mg mL^{-1} AuNP) and Au-PDMS-NH_3^+PSS (0.1 mg mL^{-1} PDMS-NH_3^+, 0.06 mg mL^{-1} PSS, and 0.016 mg mL^{-1} AuNP).

X-ray Scattering. A triple area detector system from Roper Scientific was used to collect simultaneously small-angle X-ray

https://doi.org/10.1021/acs.langmuir.3c02326
Langmuir 2023, 39, 15748−15755

scattering (SAXS), mid-angle X-ray scattering (MAXS), and wide-angle X-ray scattering (WAXS) data at beamline 5-ID-D at the Advanced Photon Source. A four-module version charge-coupled device (CCD) was used as the SAXS detector (6 × 6 binning), while a two-module version CCD was used for the MAXS (4 × 4 binning) and WAXS (2 × 2 binning) detectors from Rayonix LLC. Lanthanum hexaboride, silver behenate, and glassy carbons were used to calibrate the WAXS, MAXS, and SAXS detectors at sample-to-detector distances from 0.2 m (WAXS), 1.0 m (MAXS), and 8.5 m (SAXS). At X-ray energies of 17 keV and wavelengths of 7.293 nm, the data was collected along the center axis of each sample that resulted in wavevector (q) ranges from 2.54×10^{-2} to 45 nm^{-1}.[45,46]

X-ray Data Analysis. The solvent background (water and hexane) was subtracted from the averaged SAXS/MAXS/WAXS data using RAW software.[47] The IRENA 2.7 package for Igor Pro 8.04 was used for data modeling and analysis. A unified Guinier exponential and power law fit were used to determine particle properties.[48−50]

Transmission Electron Microscopy. Scanning transmission electron microscopy (STEM) images of the Au-PDMS-NH_3^+ were collected using a JEOL JEM-ARM200cF (a cold field emission probe-corrected TEM, Peabody, MA) operating at 200 kV. The TEM grids were prepared by drop casting dilute dispersions of the Au-PDMS-NH_3^+ in a 95:5 water/THF mixture onto lacey carbon grids, followed by slow drying under a mild vacuum. Under the conditions used, TEM only observes the inorganic particles, as the electron contrast for the hydrocarbons is too low.

Contact Angle. The PDMS-NH_3^+ contact angle on polished carbon was measured with a KSV CAM 200 goniometer using the optical contact angle and surface tension software (KSV Instruments).

RESULTS AND DISCUSSION

Encapsulation of Hydrophobic Gold Nanoparticles. Oleylamine-capped gold nanoparticles as well as hydrophobic iron oxide and hydrophobic silica nanoparticles were stabilized in aqueous media by using a short polydimethylsiloxane with protonated amine ends (PDMS-$NH_3^+Tf^-$, Scheme 1). Triflic acid provided a hydrophobic counterion on protonation of PDMS-NH_2.

Scheme 1. Structures of the Surface Ligands and Polymers Used

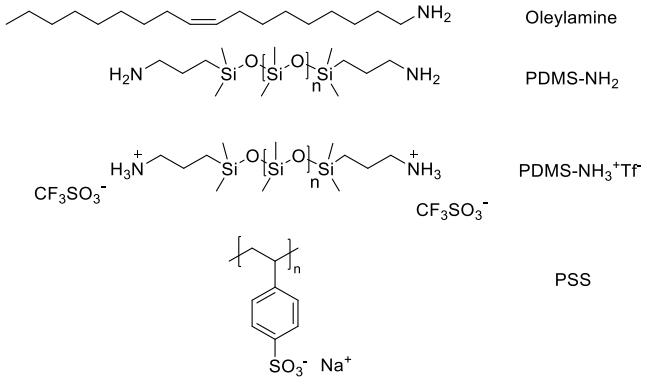

The hydrophobic AuNPs were encapsulated by PDMS-NH_3^+ using a recently reported FNP procedure.[42] The size of particles depends on a number of factors, including reactor design.[22,23] The size range, from 50 to 150 nm, is typical for FNP.[51,52] Oleylamine, widely used in the controlled preparation of capped monodisperse gold nanoparticles, simultaneously serves as a solvent and a stabilizing ligand.[43,53]

The AuNPs in hexane were dried and redispersed in a minimum amount of THF for FNP, which involved the rapid mixing of dispersed AuNPs and PDMS-$NH_3^+Tf^-$ in THF with water (a nonsolvent for both). The optimized concentration of AuNPs in the nanocomposite was found to be 0.016 mg mL^{-1} with a Au/PDMS weight ratio of 1:6.25. Various factors affecting the FNP were addressed in our previous work.[42] Here, the concentration of inorganic nanoparticles is an additional variable. For example, higher concentrations of AuNP led to larger water-dispersed composite nanodroplets.[10,19,37] AuNPs were found to self-assemble or form loose aggregates when left for a longer period of time in THF or when larger THF volumes were used.[54] Figure S4 shows an increase in the hydrodynamic radius of AuNPs in THF after 24 h, while Figure S5 shows a broadening and red shifting of the SPR peak, indicating aggregation.[54] The opposite was observed when the AuNPs were encapsulated in the PDMS-NH_3^+ nanocomposite. The composite nanodroplets had an average hydrodynamic radius of 26.5 nm (Figure 1A), a narrow SPR peak at 522 nm (Figure 1B), and remained stable for at least 24 h. However, these CNPs aggregated in the presence of salt.[42] With the addition of PSS to the surface, the R_h of the composite nanodroplet increased to 51.5 nm (Figure 1A). This increase in radius was not a sign of internal instability within the PDMS since a narrow SPR peak at 523 nm (Figure 1B) remained stable for 24 h (Figure S3), which is comparable to stable AuNPs in solution. This indicates that the AuNPs maintain a sufficient large interparticle distance within hydrophobic PDMS at the optimized AuNP concentration.[31,37] The PSS shell stabilizes hydrophobic PDMS nanodroplets but also bridges some of them. The UV−vis spectra of samples with and without gold nanoparticles showed that neither the PDMS-NH_3^+ nor the PSS contribute to the absorption in the region of the SPR peak (Figures 1B and S8).

To obtain stable, uniform, and high-loading nanodroplets via FNP, several factors must be considered. One key state is supersaturation, at which particle nucleation is induced. Large, polydisperse, unstable particles precipitate and settle if supersaturation is not achieved.[51,52] Figure S6 shows nanodroplets of size 111 nm that increase to 208 nm when prepared by FNP using only 0.1 mg mL^{-1} PDMS-NH_3^+ (without AuNP). This suggests that a low polymer concentration favors the growth of the particle instead of its nucleation.[51,52] The AuNPs act as seeding agents, inducing small, stable PDMS-NH_3^+ nanodroplets (Scheme 2). The hydrophobic nature of the AuNPs is necessary for particle formation at a PDMS-NH_3^+ concentration of 0.1 mg mL^{-1}.[51] This mechanism was also seen when comparing the hydrodynamic radius of the Au-PDMS-NH_3^+PSS and PDMS-NH_3^+PSS samples, both having equal concentrations of PSS and PDMS-NH_3^+. After 24 h, the 55 nm initial PSS-PDMS-NH_3^+ sample was not stable, and its size increased to 77 nm (Figure S7, Supporting Information). The AuNP initiated particle formation allowed a high load concentration of AuNP. The optimized AuNP concentration controlled the distance between the AuNP, preventing aggregation.[37]

Assembly of Encapsulated Gold Nanoparticles. Assembly of nanoparticles into higher-order structures has been studied using small-angle scattering[55−58] and transmission electron microscopy (TEM). Surface modification has been used to control interparticle interactions by allowing or preventing aggregation.[55] Thus, interactions between particles can be classified as repulsive and stabilizing or attractive and destabilizing. The SAXS data in Figure 2 presents the characteristic profile of the concentrated OLA-AuNP dis-

https://doi.org/10.1021/acs.langmuir.3c02326
Langmuir 2023, 39, 15748−15755

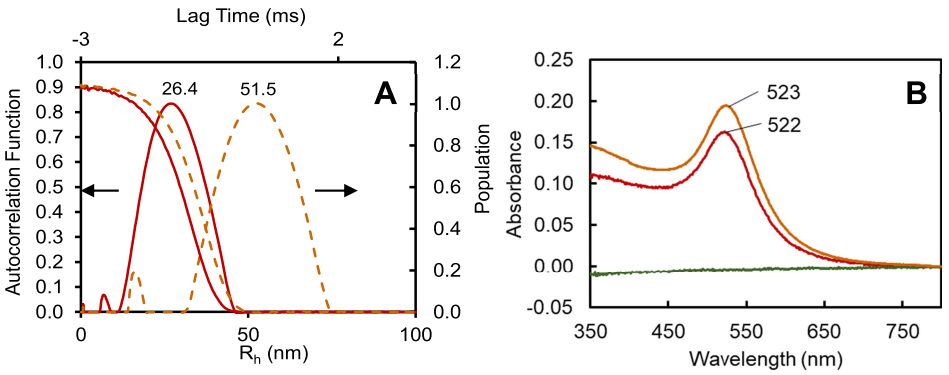

Figure 1. (A) Autocorrelation function and hydrodynamic radius, R_h, distribution of 0.1 mg mL^{-1} nanodroplets of Au-PDMS-NH$_3^+$ (0.016 mg mL^{-1} AuNP) (red —) and Au-PDMS-NH$_3^+$ PSS (0.016 mg mL^{-1} AuNP and 0.06 mg mL^{-1} PSS) (orange --) 95:5 water/THF at 296.8 K. (B) UV−vis absorbance vs wavelength of 0.1 mg mL^{-1} Au-PDMS-NH$_3^+$ (red —) (SPR peak at 522 nm), Au-PDMS-NH$_3^+$ PSS (orange —) (SPR peak at 523 nm), and PDMS-NH$_3^+$ (green —) as a control.

Scheme 2. Nanodroplet Formation at 0.1 mg mL^{-1} PDMS-NH$_3^+$ in the Presence (A) and Absence (B) of AuNP; The AuNPs Are Needed for Nanodroplet Nucleation at This Polymer Concentration

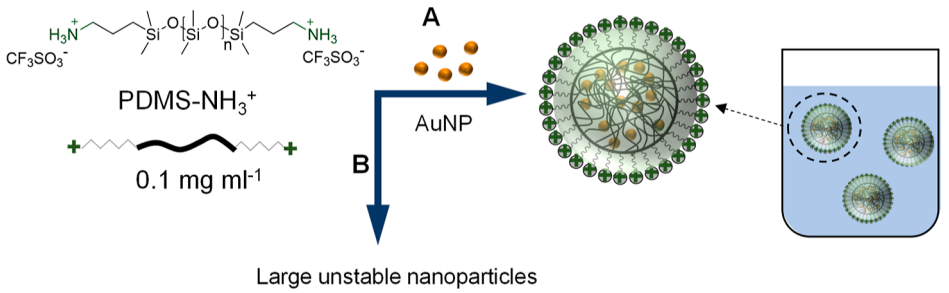

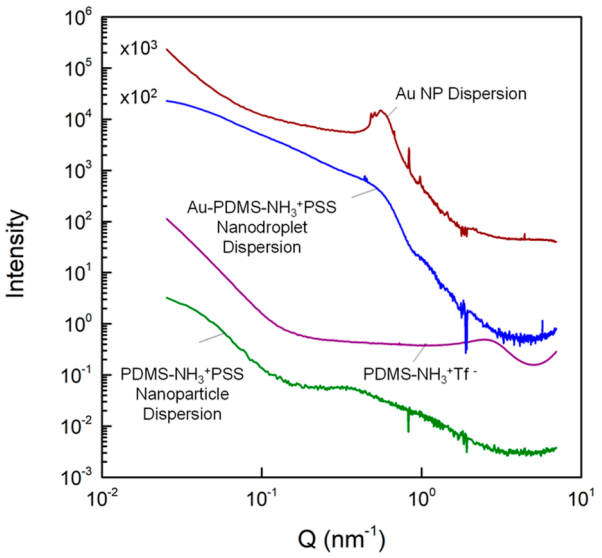

Figure 2. Small- and mid-angle X-ray scattering profiles of 1.2 × 10^{-5} wt % AuNP dispersion in hexane, Au-PDMS-NH$_3^+$PSS 0.5 wt % nanodroplet dispersion, bulk PDMS-NH$_3^+$Tf$^-$ and PDMS-NH$_3^+$PSS 1 wt % nanoparticle dispersion (top to bottom). AuNP dispersion and Au-PDMS-NH$_3^+$PSS 0.5 wt % nanodroplet dispersion curves are shifted upward for clarity. Data for PDMS-NH$_3^+$Tf$^-$ and PDMS-NH$_3^+$PSS 1 wt % nanodroplet dispersion are from ref 42.

persion in hexane and the micelle peak of the pure bulk PDMS-NH$_3^+$Tf$^-$ that appears at 2.66 nm^{-1}.[42] The PSS peak between 0.18 and 2.75 nm^{-1} in the PDMS-NH$_3^+$PSS SAXS profile[42] (Figure 2) is overwhelmed by scattering from the AuNP. It is assumed that the PSS would act as a bridge between the positively charged nanodroplets (Scheme 3), as observed in the PDMS-NH$_3^+$PSS nanocomposite.[42] A unified law by Beaucage was implemented to capture the hierarchical structures in solutions ranging from a single aggregate to several fractal aggregates coexisting on different size scales.[49,55,59]

A 0.1 mg mL^{-1} Au-PDMS-NH$_3^+$ PSS nanodroplet dispersion was passed through a 0.1 μm filter and concentrated to 5 mg mL^{-1}. The hydrodynamic radius of the nanodroplets in the more concentrated solution remained the same and stable. No residual isolated AuNPs were detected. The SAXS profiles correspond to an aggregated system formed from loose aggregates with a scattering intensity mainly determined by the gold nanoparticles.[57,60] This system is characterized by a slope of −2 at low q and a radius of gyration, R_g, of 37.2 nm (Figure 3, Table S1), which correlates to the (somewhat larger) hydrodynamic radius determined by DLS in Figure 1A.[57,60] The AuNPs imbedded within PDMS-NH$_3^+$ have an interparticle center-to-center distance (Scheme 3, Table S1) of 4.8 nm, represented by the peak at 0.53 nm^{-1} (Figure 3). At q > 1 nm^{-1}, the scattering intensity is governed by a single nanoparticle having a slope of −4 characteristic of a hard sphere and an average R_g of 2.9 nm (Scheme 3, Table S1), similar to the size of a single Au nanoparticle determined by TEM (4.3 ± 1.3 nm, Figure 4).[55]

The characteristic *hkl* peaks of gold nanoparticles are present in the WAXS spectrum in Figure S9 at the same 2θ values (24.5, 28.1, and 40.6°) in the hexane and the encapsulated samples. The peaks have not shifted, but the intensity has decreased due to the lower concentration in the encapsulated

https://doi.org/10.1021/acs.langmuir.3c02326
Langmuir 2023, 39, 15748−15755

Scheme 3. Composite Nanodroplet Network with PSS Acting as a Bridge between the Positively Charged PDMS Nanodroplets[42a]

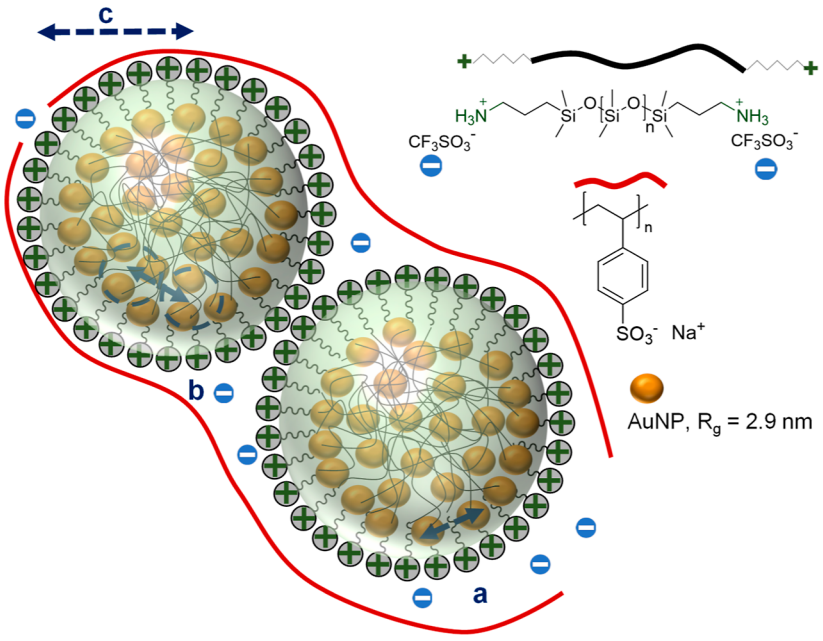

[a]37.2 nm corresponds to the size of the AuNP mass fractal encapsulated within the PDMS core. The interparticle center-to-center distance of 4.8 nm of the AuNPs is loosely assembled and embedded in the PDMS core. 2.9 nm is the average R_g of the smallest component: a single gold nanoparticle separated by 5.7 nm. The distances "**a**" (5.7 nm, Table S1), "**b**" (4.8 nm, Table S1), and "**c**" (37.2 nm, Figure 3) are deduced by X-ray scattering. The green depicts the Tf^- counterions remaining within the NP to balance the positive charge of the PDMS-NH_3^+

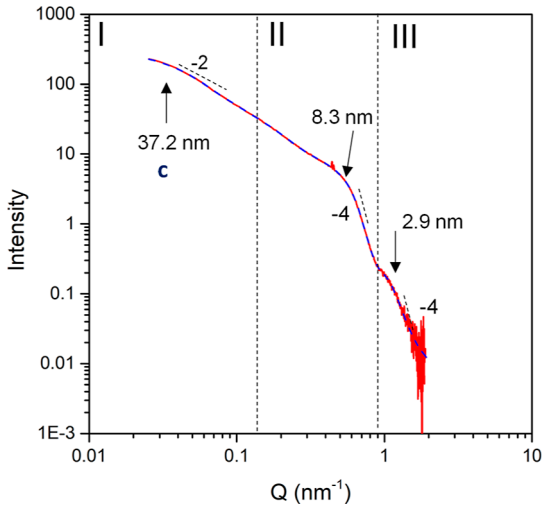

Figure 3. SAXS profile (red —) and unified fit model (blue --) of the Au-PDMS-NH_3^+PSS 0.5 wt % nanodroplet, with "**c**" being the R_g of the mass fractal of AuNP embedded within the PDMS core. The individual fits for populations **I**, **II**, and **III** are represented in Figure S10.

samples. This confirms that the AuNP remained intact upon encapsulation.

TEM samples were prepared from the Au-PDMS-NH_3^+ nanodroplet dispersion with a PDMS-NH_3^+ concentration of 0.1 mg mL^{-1}. The TEM images in Figure 4 show the gold nanoparticles assembled in a ring-like morphology around the edges of the PDMS-NH_3^+ nanodroplet. This phenomenon can be explained by using contact angle measurements. When a drop of PDMS-NH_2 touches a carbon surface of composition like that of the TEM grid, an angle of 25° is formed (Figure S11). A contact angle smaller than 90° indicates that the polymer wets the surface and spreads. Thus, the AuNPs encapsulated in the PDMS-NH_3^+ will flow as PDMS spreads. Other images (Figure 4C) show that sometimes not all of the AuNP is drawn out the edge of the PDMS as it spreads.

These PDMS-NH_3^+ nanodroplets hold an average of about 150 hydrophobically capped gold nanoparticles, describing them as high-loading nanocarriers. The AuNPs are closely packed and separated by a 3 nm gap, which is less than the distance predicted by the plasmon ruler. According to the "plasmon ruler equation," AuNPs should be separated by a distance of at least of 1.5*D* (where *D* is the diameter of the nanoparticle) to prevent a shift in the surface plasmon peak.[61] This gap is decreased in the presence of a polymer layer.[62]

The X-ray scattering analysis of the nanodroplet self-assembly represents a more 3D spherical shape compared to the flattened structures represented in TEM. The difference in morphology is due to the presence of the glassy PSS shell.[42] The gold nanoparticles form aggregates in the CIJ-D mixer upon contact with water, which are consequently stabilized by the PDMS-NH_3^+ and the PSS shell.[31]

Encapsulation of Other Inorganic NPs. To illustrate the generality of the encapsulation method, PDMS-NH_3^+ nanodroplets were loaded with other inorganic core chemistries: hydrophobic iron oxide and hydrophobic silica nanoparticles. The optimal concentration of iron oxide was determined to be 0.032 mg mL^{-1}; lower concentrations created aggregation-prone nanodroplets.[51] The iron oxide nanoparticles were dried from hexane, redispersed in 10 mL of THF, sonicated for 10 min, and passed through a 0.2 μm filter before mixing with the PDMS solution. The hydrodynamic radius of the particles remained stable at 12 nm for 24 h (Figure S13). For the SiO_2 NPs, drying from IPA was not a suitable option. The silica NPs

https://doi.org/10.1021/acs.langmuir.3c02326
Langmuir 2023, 39, 15748−15755

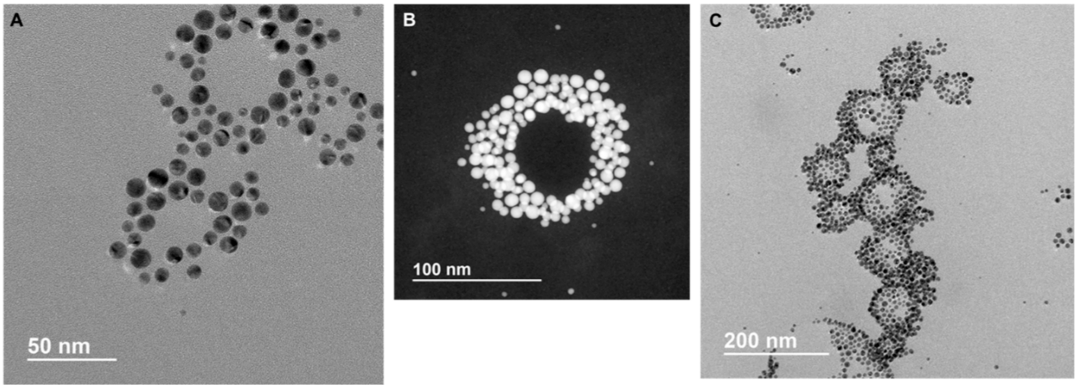

Figure 4. TEM images of a 0.1 mg mL^{-1} Au-PDMS-NH_3^+ nanodroplets at different magnifications from (A) to (C). Annual-dark-field STEM image (B) shows 146 gold nanoparticles (in white) clustered in a ring. AuNP radius: 4.7 ± 1.5 nm.

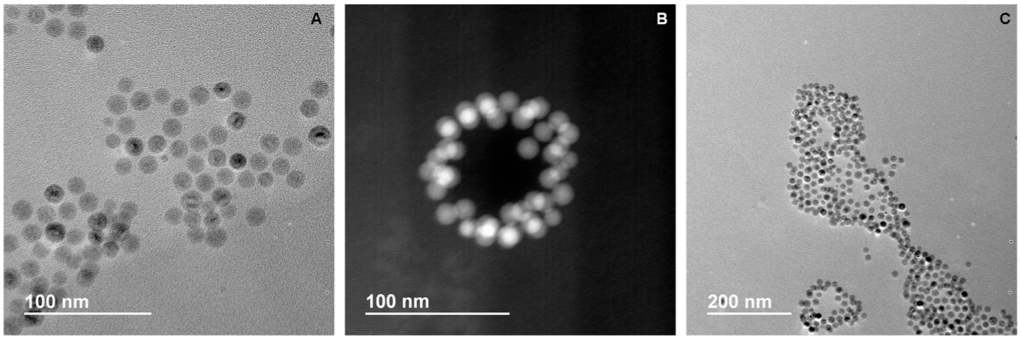

Figure 5. TEM images of 0.1 mg mL^{-1} IONP-PDMS-NH_3^+ nanodroplets at different magnifications from (A) to (C). Annual-dark-field STEM image (B) shows 43 iron oxide nanoparticles (in white) clustered in a ring. IONP radius 7.4 ± 1.6 nm.

were instead used as a suspension and dispersed in THF. The hydrodynamic radius in THF was around 12 nm (Figure S15), comparable to the size stated by the manufacturer. The IONP-PDMS-NH_3^+ and SiO_2 NP-PDMS-NH_3^+ were then prepared using the same FNP technique as that mentioned above. The hydrodynamic radius was around 38 and 33 nm for the IONP-PDMS-NH_3^+ and SiO_2 NP-PDMS-NH_3^+ nanodroplets, respectively (Supporting Information, Figures S14 and S16). The three different inorganic cores formed PDMS-NH_3^+ nanodroplets with almost the same size, indicating that the nucleation mechanism discussed above applies to a variety of inorganic particles. The positively charged nanocarriers were stabilized in an aqueous solution for at least 24 h.

The TEM images shown in Figures 5 and S16 show the iron oxide and silica nanoparticles assembled in a ring-like morphology around the edges of the PDMS-NH_3^+ nanodroplet, similar to the gold nanoparticles in Figure 4. The loading decreased to 43 and 19 nanoparticles due to the increase in size of the IONP and SiO_2, respectively.

CONCLUSIONS

PDMS with positively charged end groups was used to make hydrophobic nanodroplets with hydrophilic shells to encapsulate various inorganic nanoparticles. Gold, iron oxide, and hydrophobically modified silica nanoparticles that tend to aggregate in aqueous solutions were protected and encapsulated at a high concentration within the hydrophobic core. These inorganic-polysiloxane composite nanodroplets can be further stabilized without the use of surfactants by forming a glassy PSS shell on the surface. To the best of our knowledge, these are the only reported stable nanocomposite PDMS nanodroplets in water. This system paves the way for new stable aqueous nanocarriers with high loading capacities for hydrophobic molecules and nanomaterials. These inorganic NP-loaded polymer nanodroplets have potential utility as hydrophobic drug carriers and contrast agents and as vehicles for catalysts. By introduction of various functionalities into the polyelectrolyte shell, the composite NPs may be targeted to specific substrates.

ASSOCIATED CONTENT

Supporting Information

The Supporting Information is available free of charge at https://pubs.acs.org/doi/10.1021/acs.langmuir.3c02326.

Photograph of CIJ mixer; dynamic light scattering of nanoparticle dispersions in water; UV−vis absorbance spectroscopy of Au-containing nanodroplets; wide-angle X-ray scattering of Au-containing nanodroplets; fit of the SAXS profile broken down according to contributions from various populations; SAXS fitting parameters using the unified fit model; contact angle of PDMS-NH_3^+ on glassy carbon; and TEM images of nanodroplets encapsulating SiO_2 (PDF)

AUTHOR INFORMATION

Corresponding Author

Joseph B. Schlenoff − *Department of Chemistry and Biochemistry, The Florida State University, Tallahassee, Florida 32306, United States;* orcid.org/0000-0001-5588-1253; Email: jschlenoff@fsu.edu

https://doi.org/10.1021/acs.langmuir.3c02326
Langmuir 2023, 39, 15748−15755

Authors

Sandrine Lteif − *Department of Chemistry and Biochemistry, The Florida State University, Tallahassee, Florida 32306, United States;* orcid.org/0000-0002-1955-1625

Neda A. Nosratabad − *Department of Chemistry and Biochemistry, The Florida State University, Tallahassee, Florida 32306, United States*

Sisi Wang − *Department of Chemistry and Biochemistry, The Florida State University, Tallahassee, Florida 32306, United States*

Yan Xin − *National High Magnetic Field Laboratory, Tallahassee, Florida 32310, United States*

Steven J. Weigand − *DND-CAT Synchrotron Research Center, Northwestern University, Argonne, Illinois 60439, United States*

Hedi Mattoussi − *Department of Chemistry and Biochemistry, The Florida State University, Tallahassee, Florida 32306, United States;* orcid.org/0000-0002-6511-9323

Complete contact information is available at: https://pubs.acs.org/10.1021/acs.langmuir.3c02326

Notes

The authors declare no competing financial interest.

■ ACKNOWLEDGMENTS

This work was supported by grants from the National Science Foundation DMR-1809304 and CHE-2005079, and Kasei-Asahi Corporation. The TEM work was performed at the National High Magnetic Field Laboratory, which is supported by National Science Foundation Cooperative Agreement DMR-1644779, DMR-1839796, DMR-2131790, and the State of Florida.

■ REFERENCES

(1) Jones, M. C.; Leroux, J. C. Polymeric Micelles-a New Generation of Colloidal Drug Carriers. *Eur. J. Pharm. Biopharm.* **1999**, *48*, 101−111.

(2) Begines, B.; Ortiz, T.; Pérez-Aranda, M.; Martínez, G.; Merinero, M.; Argüelles-Arias, F.; Alcudia, A. Polymeric Nanoparticles for Drug Delivery: Recent Developments and Future Prospects. *Nanomaterials* **2020**, *10*, 1403.

(3) Gindy, M. E.; Panagiotopoulos, A. Z.; Prud'homme, R. K. Composite Block Copolymer Stabilized Nanoparticles: Simultaneous Encapsulation of Organic Actives and Inorganic Nanostructures. *Langmuir* **2008**, *24*, 83−90.

(4) Hornig, S.; Heinze, T.; Becer, C. R.; Schubert, U. S. Synthetic Polymeric Nanoparticles by Nanoprecipitation. *J. Mater. Chem.* **2009**, *19*, 3838−3840.

(5) Zielińska, A.; Carreiró, F.; Oliveira, A. M.; Neves, A.; Pires, B.; Venkatesh, D. N.; Durazzo, A.; Lucarini, M.; Eder, P.; Silva, A. M.; et al. Polymeric Nanoparticles: Production, Characterization, Toxicology and Ecotoxicology. *Molecules* **2020**, *25*, 3731.

(6) Nejati, K.; Dadashpour, M.; Gharibi, T.; Mellatyar, H.; Akbarzadeh, A. Biomedical Applications of Functionalized Gold Nanoparticles: A Review. *J. Cluster Sci.* **2021**, *33*, 1−16.

(7) Van der Ven, C. F.; Tibbitt, M. W.; Conde, J.; Van Mil, A.; Hjortnaes, J.; Doevendans, P. A.; Sluijter, J. P.; Aikawa, E.; Langer, R. S. Controlled Delivery of Gold Nanoparticle-Coupled MiRNA Therapeutics Via an Injectable Self-Healing Hydrogel. *Nanoscale* **2021**, *13*, 20451−20461.

(8) Oh, E.; Susumu, K.; Goswami, R.; Mattoussi, H. One-Phase Synthesis of Water-Soluble Gold Nanoparticles with Control over Size and Surface Functionalities. *Langmuir* **2010**, *26*, 7604−7613.

(9) Mei, B. C.; Susumu, K.; Medintz, I. L.; Mattoussi, H. Polyethylene Glycol-Based Bidentate Ligands to Enhance Quantum Dot and Gold Nanoparticle Stability in Biological Media. *Nat. Protoc.* **2009**, *4*, 412−423.

(10) Shen, H.; Hong, S.; Prud'homme, R. K.; Liu, Y. Self-Assembling Process of Flash Nanoprecipitation in a Multi-Inlet Vortex Mixer to Produce Drug-Loaded Polymeric Nanoparticles. *J. Nanopart. Res.* **2011**, *13*, 4109−4120.

(11) Owen, S. C.; Chan, D. P.; Shoichet, M. S. Polymeric Micelle Stability. *Nano Today* **2012**, *7*, 53−65.

(12) Rao, J. P.; Geckeler, K. E. Polymer Nanoparticles: Preparation Techniques and Size-Control Parameters. *Prog. Polym. Sci.* **2011**, *36*, 887−913.

(13) Hu, S.; Yan, J.; Yang, G.; Ma, C.; Yin, J. Self-Assembled Polymeric Materials: Design, Morphology, and Functional-Oriented Applications. *Macromol. Rapid Commun.* **2022**, *43*, No. e2100791.

(14) Nagavarma, B.; Yadav, H. K.; Ayaz, A.; Vasudha, L.; Shivakumar, H. Different Techniques for Preparation of Polymeric Nanoparticles-a Review. *Asian J. Pharm. Clin. Res.* **2012**, *5*, 16−23.

(15) Yu, Q.; Sun, N.; Hu, D.; Wang, Y.; Chang, X.; Yan, N.; Zhu, Y.; Li, Y. Encapsulation of Inorganic Nanoparticles in a Block Copolymer Vesicle Wall Driven by the Interfacial Instability of Emulsion Droplets. *Polym. Chem.* **2021**, *12*, 4184−4192.

(16) Nabar, G. M.; Winter, J. O.; Wyslouzil, B. E. Nanoparticle Packing within Block Copolymer Micelles Prepared by the Interfacial Instability Method. *Soft Matter* **2018**, *14*, 3324−3335.

(17) Alkilany, A. M.; Abulateefeh, S. R.; Murphy, C. J. Facile Functionalization of Gold Nanoparticles with Plga Polymer Brushes and Efficient Encapsulation into Plga Nanoparticles: Toward Spatially Precise Bioimaging of Polymeric Nanoparticles. *Part. Part. Syst. Charact.* **2019**, *36*, 1800414.

(18) Bae, J.; Lawrence, J.; Miesch, C.; Ribbe, A.; Li, W.; Emrick, T.; Zhu, J.; Hayward, R. C. Multifunctional Nanoparticle-Loaded Spherical and Wormlike Micelles Formed by Interfacial Instabilities. *Adv. Mater.* **2012**, *24*, 2735−2741.

(19) Park, J. H.; von Maltzahn, G.; Ruoslahti, E.; Bhatia, S. N.; Sailor, M. J. Micellar Hybrid Nanoparticles for Simultaneous Magnetofluorescent Imaging and Drug Delivery. *Angew. Chem.* **2008**, *120*, 7394−7398.

(20) Dubertret, B.; Skourides, P.; Norris, D. J.; Noireaux, V.; Brivanlou, A. H.; Libchaber, A. In Vivo Imaging of Quantum Dots Encapsulated in Phospholipid Micelles. *Science* **2002**, *298*, 1759−1762.

(21) Johnson, B. K.; Prud'homme, R. K. Flash Nanoprecipitation of Organic Actives and Block Copolymers Using a Confined Impinging Jets Mixer. *Aust. J. Chem.* **2003**, *56*, 1021−1024.

(22) Han, J.; Zhu, Z.; Qian, H.; Wohl, A. R.; Beaman, C. J.; Hoye, T. R.; Macosko, C. W. A Simple Confined Impingement Jets Mixer for Flash Nanoprecipitation. *J. Pharm. Sci.* **2012**, *101*, 4018−4023.

(23) Pustulka, K. M.; Wohl, A. R.; Lee, H. S.; Michel, A. R.; Han, J.; Hoye, T. R.; McCormick, A. V.; Panyam, J.; Macosko, C. W. Flash Nanoprecipitation: Particle Structure and Stability. *Mol. Pharmaceutics* **2013**, *10*, 4367−4377.

(24) Johnson, B. K.; Prud'homme, R. K. Chemical Processing and Micromixing in Confined Impinging Jets. *AIChE J.* **2003**, *49*, 2264−2282.

(25) Levit, S. L.; Walker, R. C.; Tang, C. Rapid, Single-Step Protein Encapsulation Via Flash Nanoprecipitation. *Polymers* **2019**, *11*, 1406.

(26) Akbulut, M.; Ginart, P.; Gindy, M. E.; Theriault, C.; Chin, K. H.; Soboyejo, W.; Prud'homme, R. K. Generic Method of Preparing Multifunctional Fluorescent Nanoparticles Using Flash Nanoprecipitation. *Adv. Funct. Mater.* **2009**, *19*, 718−725.

(27) Pansare, V. J.; Bruzek, M. J.; Adamson, D. H.; Anthony, J.; Prud'homme, R. K. Composite Fluorescent Nanoparticles for Biomedical Imaging. *Mol. Imaging Biol.* **2014**, *16*, 180−188.

(28) Kudisch, B.; Maiuri, M.; Wang, L.; Lim, T.; Lu, H.; Lee, V.; Prud'homme, R. K.; Scholes, G. D. Binary Small Molecule Organic Nanoparticles Exhibit Both Direct and Diffusion-Limited Ultrafast Charge Transfer with NIR Excitation. *Nanoscale* **2019**, *11*, 2385−2392.

(29) Ansell, S. M.; Johnstone, S. A.; Tardi, P. G.; Lo, L.; Xie, S.; Shu, Y.; Harasym, T. O.; Harasym, N. L.; Williams, L.; Bermudes, D.; et al. Modulating the Therapeutic Activity of Nanoparticle Delivered Paclitaxel by Manipulating the Hydrophobicity of Prodrug Conjugates. *J. Med. Chem.* **2008**, *51*, 3288−3296.
(30) Shen, L.; Wang, T.; Goyal, S.; Lee, T. H.; Lin, F. Y.; Torres, S.; Robison, T.; Cochran, E. W. Easy-Processable and Aging-Free All-Polymer Polysiloxane Composites. *ACS Appl. Polym. Mater.* **2020**, *2*, 5835−5844.
(31) Zhang, Y.; Clapp, A. R. Preparation of Quantum Dot-Embedded Polymeric Nanoparticles Using Flash Nanoprecipitation. *RSC Adv.* **2014**, *4*, 48399−48410.
(32) Fu, Z.; Chen, K.; Li, L.; Zhao, F.; Wang, Y.; Wang, M.; Shen, Y.; Cui, H.; Liu, D.; Guo, X. Spherical and Spindle-Like Abamectin-Loaded Nanoparticles by Flash Nanoprecipitation for Southern Root-Knot Nematode Control: Preparation and Characterization. *Nanomaterials* **2018**, *8*, 449.
(33) Budijono, S. J.; Shan, J.; Yao, N.; Miura, Y.; Hoye, T.; Austin, R. H.; Ju, Y.; Prud'homme, R. K. Synthesis of Stable Block-Copolymer-Protected $NaYF_4$: Yb^{3+}, Er^{3+} Up-Converting Phosphor Nanoparticles. *Chem. Mater.* **2010**, *22*, 311−318.
(34) Qian, H.; Wohl, A. R.; Crow, J. T.; Macosko, C. W.; Hoye, T. R. A Strategy for Control of "Random" Copolymerization of Lactide and Glycolide: Application to Synthesis of PEG-B-PLGA Block Polymers Having Narrow Dispersity. *Macromolecules* **2011**, *44*, 7132−7140.
(35) Mares, A. G.; Pacassoni, G.; Marti, J. S.; Pujals, S.; Albertazzi, L. Formulation of Tunable Size PLGA-PEG Nanoparticles for Drug Delivery Using Microfluidic Technology. *PLoS One* **2021**, *16*, No. e0251821.
(36) Zheng, C. Gradient Copolymer Micelles: An Introduction to Structures as Well as Structural Transitions. *Soft Matter* **2019**, *15*, 5357−5370.
(37) Reisch, A.; Trofymchuk, K.; Runser, A.; Fleith, G.; Rawiso, M.; Klymchenko, A. S. Tailoring Fluorescence Brightness and Switching of Nanoparticles through Dye Organization in the Polymer Matrix. *ACS Appl. Mater. Interfaces* **2017**, *9*, 43030−43042.
(38) Reisch, A.; Runser, A.; Arntz, Y.; Mely, Y.; Klymchenko, A. S. Charge-Controlled Nanoprecipitation as a Modular Approach to Ultrasmall Polymer Nanocarriers: Making Bright and Stable Nanoparticles. *ACS Nano* **2015**, *9*, 5104−5116.
(39) Zhao, W.; Fonsny, P.; FitzGerald, P.; Warr, G. G.; Perrier, S. Unexpected Behavior of Polydimethylsiloxane/Poly(2-(Dimethylamino) Ethyl Acrylate)(Charged) Amphiphilic Block Copolymers in Aqueous Solution. *Polym. Chem.* **2013**, *4*, 2140−2150.
(40) Car, A.; Baumann, P.; Duskey, J. T.; Chami, M.; Bruns, N.; Meier, W. pH-Responsive PDMS-*b*-PDMAEMA Micelles for Intracellular Anticancer Drug Delivery. *Biomacromolecules* **2014**, *15*, 3235−3245.
(41) Maparu, A. K.; Singh, P.; Rai, B.; Sharma, A.; Sivakumar, S. Stable Sub-100 nm PDMS Nanoparticles as an Intracellular Drug Delivery Vehicle. *Mater. Sci. Eng., C* **2021**, *119*, 111577.
(42) Lteif, S.; Akkaoui, K.; Abou Shaheen, S.; Chaaban, M.; Weigand, S.; Schlenoff, J. B. Gummy Nanoparticles with Glassy Shells in Electrostatic Nanocomposites. *Langmuir* **2022**, *38*, 9611−9620.
(43) Liu, S.; Chen, G.; Prasad, P. N.; Swihart, M. T. Synthesis of Monodisperse Au, Ag, and Au-Ag Alloy Nanoparticles with Tunable Size and Surface Plasmon Resonance Frequency. *Chem. Mater.* **2011**, *23*, 4098−4101.
(44) Park, J.; An, K.; Hwang, Y.; Park, J. G.; Noh, H. J.; Kim, J. Y.; Park, J. H.; Hwang, N.-M.; Hyeon, T. Ultra-Large-Scale Syntheses of Monodisperse Nanocrystals. *Nat. Mater.* **2004**, *3*, 891−895.
(45) Weigand, S. J.; Keane, D. T. DND-CAT's New Triple Area Detector System for Simultaneous Data Collection at Multiple Length Scales. *Nucl. Instrum. Methods Phys. Res., Sect. A* **2011**, *649*, 61−63.
(46) Weigand, S.; Stillwell, B.; Guise, W. E.; Quintana, J. P.; Keane, D. T. Flexibility and High Throughput: Supporting SAXS Users at a Joint Industrial Academic Beamline. *Adv. X-Ray Anal.* **2009**, *52*, 58−68.
(47) Hopkins, J. B.; Gillilan, R. E.; Skou, S. Bioxtas RAW: Improvements to a Free Open-Source Program for Small-Angle X-Ray Scattering Data Reduction and Analysis. *J. Appl. Crystallogr.* **2017**, *50*, 1545−1553.
(48) Ilavsky, J.; Jemian, P. R. Irena: Tool Suite for Modeling and Analysis of Small-Angle Scattering. *J. Appl. Crystallogr.* **2009**, *42*, 347−353.
(49) Beaucage, G. Approximations Leading to a Unified Exponential/Power-Law Approach to Small-Angle Scattering. *J. Appl. Crystallogr.* **1995**, *28*, 717−728.
(50) Anitas, E. M. Small-Angle Scattering from Weakly Correlated Nanoscale Mass Fractal Aggregates. *Nanomaterials* **2019**, *9*, 648.
(51) Saad, W. S.; Prud'homme, R. K. Principles of Nanoparticle Formation by Flash Nanoprecipitation. *Nano Today* **2016**, *11*, 212−227.
(52) Liu, Y.; Yang, G.; Zou, D.; Hui, Y.; Nigam, K.; Middelberg, A. P.; Zhao, C. X. Formulation of Nanoparticles Using Mixing-Induced Nanoprecipitation for Drug Delivery. *Ind. Eng. Chem. Res.* **2020**, *59*, 4134−4149.
(53) Mourdikoudis, S.; Liz-Marzán, L. M. Oleylamine in Nanoparticle Synthesis. *Chem. Mater.* **2013**, *25*, 1465−1476.
(54) Liu, X.; Atwater, M.; Wang, J.; Dai, Q.; Zou, J.; Brennan, J. P.; Huo, Q. A Study on Gold Nanoparticle Synthesis Using Oleylamine as Both Reducing Agent and Protecting Ligand. *J. Nanosci. Nanotechnol.* **2007**, *7*, 3126−3133.
(55) Genix, A.-C.; Bocharova, V.; Kisliuk, A.; Carroll, B.; Zhao, S.; Oberdisse, J.; Sokolov, A. P. Enhancing the Mechanical Properties of Glassy Nanocomposites by Tuning Polymer Molecular Weight. *ACS Appl. Mater. Interfaces* **2018**, *10*, 33601−33610.
(56) Chen, X.; Schroder, J.; Hauschild, S.; Rosenfeldt, S.; Dulle, M.; Forster, S. Simultaneous SAXS/WAXS/Uv-Vis Study of the Nucleation and Growth of Nanoparticles: A Test of Classical Nucleation Theory. *Langmuir* **2015**, *31*, 11678−11691.
(57) Mulderig, A.; Beaucage, G.; Vogtt, K.; Jiang, H.; Jin, Y.; Clapp, L.; Henderson, D. C. Structural Emergence in Particle Dispersions. *Langmuir* **2017**, *33*, 14029−14037.
(58) Genix, A. C.; Oberdisse, J. Nanoparticle Self-Assembly: From Interactions in Suspension to Polymer Nanocomposites. *Soft Matter* **2018**, *14*, 5161−5179.
(59) Beaucage, G. Determination of Branch Fraction and Minimum Dimension of Mass-Fractal Aggregates. *Phys. Rev. E: Stat., Nonlinear, Soft Matter Phys.* **2004**, *70*, 031401.
(60) Moro, S.; Parneix, C.; Cabane, B.; Sanson, N.; d'Espinose de Lacaillerie, J.-B. Hydrophobization of Silica Nanoparticles in Water: Nanostructure and Response to Drying Stress. *Langmuir* **2017**, *33*, 4709−4719.
(61) Jain, P. K.; Huang, W.; El-Sayed, M. A. On the Universal Scaling Behavior of the Distance Decay of Plasmon Coupling in Metal Nanoparticle Pairs: A Plasmon Ruler Equation. *Nano Lett.* **2007**, *7*, 2080−2088.
(62) Grady, N. K.; Knight, M. W.; Bardhan, R.; Halas, N. J. Optically-Driven Collapse of a Plasmonic Nanogap Self-Monitored by Optical Frequency Mixing. *Nano Lett.* **2010**, *10*, 1522−1528.

https://doi.org/10.1021/acs.langmuir.3c02326
Langmuir 2023, 39, 15748−15755